Exploring necroptosis-associated genes: implications for immune responses and therapeutic strategies in diabetic foot ulcers

Keywords
biomarkers, bioinformatics analysis, necroptosis, diabetic foot ulcer

Abstract

Introduction
Diabetic foot ulcers (DFUs) are among the most severe and debilitating diabetic complications, often leading to extremely high morbidity and mortality. Recently, increasing evidence has highlighted the role of necroptosis, a distinct type of programmed cell death distinct from apoptosis, in the progression and severity of DFUs. Understanding necroptosis-associated genes in DFUs could open new therapeutic avenues aimed at modulating this form of cell death, potentially improving outcomes for patients suffering from this serious diabetic complication.

Material and methods
This study focuses on discovering and confirming potential necroptosis biomarkers linked to DFU through the application of machine learning and bioinformatics approaches. We obtained three microarray datasets associated with DFU individuals from the Gene Expression Omnibus (GEO) database: GSE68183, GSE134431, and GSE80178.

Results
In GSE134431, we identified necroptosis-associated genes (NRGs) with differential expression between DFU patients and healthy controls, totaling 37 NRGs. Additionally, we observed an activated immune response in both groups. Moreover, clustering analysis revealed two distinct clusters within the DFU samples, showcasing immune heterogeneity. Subsequently, we constructed a Random Forest (RF) model utilizing 5 genes (CENPB, TRIM56, ZNF768, PLIN4, and ATP1A1). Notably, this model demonstrated outstanding performance on the external validation datasets GSE134431, GSE68183 (AUC = 1.000). The study has pinpointed five genes linked to necroptosis in the context of DFU, unveiling new potential biomarkers and targets for DFU therapy.

Conclusions
Bioinformatics analysis elucidated that CENPB, TRIM56, ZNF768, PLIN4, and ATP1A1 could serve as potential biomarkers for future DFU research.

Exploring necroptosis-associated genes: implications for immune responses and therapeutic strategies in diabetic foot ulcers

Meijie Yuan[1], Jian Sun[1], Zhuo Zhao[1], Xiaoming Hu[1], Weijing Fan[1]*, Hongshuo Shi[1]*, Guobin Liu[1]*

Abstract

Introduction:

Diabetic foot ulcers (DFUs) are among the most severe and debilitating diabetic complications, often leading to extremely high morbidity and mortality. Recently, increasing evidence has highlighted the role of necroptosis, a distinct type of programmed cell death distinct from apoptosis, in the progression and severity of DFUs. Understanding necroptosis-associated genes in DFUs could open new therapeutic avenues aimed at modulating this form of cell death, potentially improving outcomes for patients suffering from this serious diabetic complication.

Material and methods:

This study focused on discovering and confirming potential necroptosis biomarkers linked to DFU through the application of machine learning and bioinformatics approaches. We obtained three microarray datasets associated with DFU individuals from the Gene Expression Omnibus (GEO) database: GSE68183, GSE134431, and GSE80178.

Results:

In GSE134431, we identified necroptosis-associated genes (NRGs) with

differential expression between DFU patients and healthy controls, totaling 37 NRGs. Additionally, we observed an activated immune response in both groups. Moreover, clustering analysis revealed two distinct clusters within the DFU samples, showcasing immune heterogeneity. Subsequently, we constructed a Random Forest (RF) model utilizing 5 genes (CENPB, TRIM56, ZNF768, PLIN4, and ATP1A1). Notably, this model demonstrated outstanding performance on the external validation datasets GSE134431, GSE68183 (AUC = 1.000). The study has pinpointed five genes linked to necroptosis in the context of DFU, unveiling new potential biomarkers and targets for DFU therapy.

Conclusions:

Bioinformatics analysis elucidated that CENPB, TRIM56, ZNF768, PLIN4, and ATP1A1 could serve as potential biomarkers for future DFU research.

Keywords:

diabetic foot ulcer, necroptosis, bioinformatics analysis, biomarkers

Introduction

Diabetic foot ulcer (DFU) is a major diabetes complication that can result in serious outcomes, including infection, gangrene, amputation, and even death. DFU affects around 18.6 million patients worldwide annually[1]. Moreover, up to about 34% of individuals with type 1 or type 2 diabetes will experience a foot ulcer at some point in their lifetime[2]. Furthermore, it is concerning that around 20% of people with a diabetic foot ulcer may require a lower extremity amputation[3]. Given the increasing prevalence of diabetes and diabetic wounds, addressing the diverse factors that impede healing in diabetic wounds is essential for developing future treatment strategies. First-line therapies for DFUs typically include surgical debridement, offloading pressure from the ulcer, and managing lower extremity ischemia and foot infections[4]. Despite advancements in treatment, nonhealing DFUs remain a persistent clinical challenge. Hence, investigating the pathological mechanisms of DFUs and advancing therapeutic strategies are essential for accelerating ulcer healing and enhancing patient prognosis.

The process of healing chronic wounds in DFU that are resistant to treatment is highly intricate. Chronic inflammation hampers the healing process by affecting the immune cells' ability to fight bacteria, reducing blood flow to the wound site, damaging the basement membrane of cells, and inhibiting the production of collagen[5]. DFU wounds provide an optimal environment for the formation of biofilms, and resistance to multiple drugs along with biofilm formation are crucial factors in the development of infections in DFU[6]. After blood sugar levels rise,

reactive oxygen species (ROS) are subsequently produced, thereby increasing the generation of inflammatory mediators, degenerate pericytes, thicken the basement membrane, cause endothelial hyperplasia, reduce prostacyclin synthesis, impair blood vessel dilation, and elevate procoagulant markers. This cascade of events results in the formation of microthrombi, leading to worsened blood flow and oxygen deprivation in diabetic wounds, causing damage to local tissues[7]. Additionally, factors such as the inhibition of growth factors, disturbances in microcirculation, and age-related changes are key factors contributing to DFU[8-10]. The precise mechanism behind the resistance to healing in DFU remains unclear, which poses challenges in diagnosing and treating these conditions effectively.

Necroptosis has been identified as a novel form of genetically controlled cell death. Initially, studies on necroptosis were mainly centered around acute nervous system[11,12], cancer[13,14], and cardiovascular diseases[15]. Necroptosis is a self-destructive cellular process that occurs when apoptosis is hindered. Cells undergoing necroptosis display necrotic characteristics such as plasma membrane disruption, organelle swelling, and cytolysis[16]. Necroptosis, initiated by specific stimuli and regulated via caspase-independent pathways, primarily involves the activation of mixed lineage kinase domain-like protein[17], receptor-interacting protein kinase 1 (RIPK1), and RIPK3[18]. While integrating necroptosis targeting with immunotherapy appears promising in neurological and cancer treatments, our understanding of how necroptosis influences immunogenicity and immunotherapy is still limited. Given the current lack of research, our study aims to extensively

investigate the relationship between necroptosis and immunotherapy in the context of DFU.

Several prior studies have employed the Gene Expression Omnibus (GEO) database to explore targets related to DFU[19,20], leveraging the advancements in bioinformatics and machine learning[21-23]. Therefore, we propose that necroptosis-associated genes (NRGs) are crucial in the development of DFU.

Materials and methods

The study utilized unsupervised cluster analysis to differentiate two unique clusters in the NRG expression matrix. Subsequently, a machine learning model was developed derived from the key DFU module and two WGCNA clusters[24,255], with the selection of key models based on diagnostic sensitivity[26]. The study seeks to unveil necroptosis-associated genes within immune responses and treatment strategies for DFUs [27,28]. Figure1 illustrated the flowchart of the study.

Raw data

We used datasets GSE134431, GSE80178, and GSE68183 from the GEO database. The training set was GSE134431, while GSE80178 and GSE68183 were validation sets. GSE68183 included 3 DFU samples and 3 normal skin samples, while GSE80178 contained 9 DFU samples and 3 normal skin samples[29]. GSE134431 comprised 13 DFU samples and 8 normal skin samples[30]. The NRG dataset was obtained from MSigDB, details were summarized in Table 1.

Dataset	Platform	Count	DFU	Control
GSE68183	GPL16686	6	3	3
GSE80178	GPL16686	12	9	3
GSE134431	GPL18573	21	13	8

Table 1: Dataset information.

Differentially expressed genes (DEGs) analysis

Data processing involved obtaining accurate mRNA data from transcription data using Perl-based matching and sorting techniques. Data normalization was then conducted for GSE134431.

The "limma" R package (version 3.52.4) was used to process raw gene expression matrices from the GEO database. To adjust for batch variations among GSE134431, GSE68183, and GSE80178, the SVA package was utilized.

Cluster analysis

By evaluating the cumulative distribution function curve, consensus cluster score and consistency matrix, the ideal cluster number was established, with the maximum cluster count set to k = 9 for this study.

Immune cell infiltration

The analysis of immune cell composition of DFU was conducted with CIBERSORT. Utilizing the limma package, we showcased the immune cell findings through barplots and corplots. Deconvolution *p*-values for each sample were obtained using Monte Carlo sampling in CIBERSORT. The transcriptional signature matrix representing 22 immune cells was utilized for the computational simulation, ensuring their total percentage of these 22 immune cells equaled one for each sample. We conducted 1,000 computational simulations, identifying samples with a p-value < 0.05 as statistically significant.

Enrichment analysis

The Kyoto Encyclopedia of Genes and Genomes (KEGG) and Gene Ontology (GO) were used to explore biological functions and pathways. The analysis of how differentially expressed GlnMRGs affect biological processes (BP), molecular functions (MF), and cellular components (CC) was assessed using the Gene Set Variation Analysis (GSVA) method in R. GSVA scores, derived through the "limma" R package (version 3.52.4), with a $|t \text{ value}| > 2$, were deemed significantly altered.

Co-expression gene identification

The Weighted Gene Co-Expression Network Analysis (WGCNA) method was employed to categorize genes and uncover connections of modules and traits. The co-expression network was constructed using the top 25% most variable genes from the GSE134431 dataset. Using a dynamic tree-cutting approach with a cutoff of 0.25, modules were merged. The modules showing the highest correlation between the two classification approaches were then identified and mapped.

Developing predictive models using various machine learning techniques

Cluster-specific NRGs were identified by combining WGCNA with the analysis of DEGs within gene clusters. The tool Vnnmap is utilized to illustrate overlapping genes. The "caret" R package was used to develop machine learning models for two distinct GlnMRG clusters, utilizing methods such as Generalized Linear Model (GLM), Support Vector Machine (SVM), Extreme Gradient Boosting (XGB), and Random Forest (RF). GLM modeled the expected response through a link function, allowing predictions of relationships from linear variable combinations[31]. XGB operated as a series of parallel trees, enhancing predictions iteratively with each new tree, which helped in aligning predictions closely with actual values[32]. SVM, a form of generalized linear classifier, was particularly effective for binary classification tasks using supervised learning, especially in small datasets and high-dimensional spaces[33]. Furthermore, RF combined multiple independent decision trees to enhance prediction accuracy for classification and regression tasks[34].

To analyze gene correlations in DFU, we used various clusters as response

175 variables and selected differentially expressed genes (DEGs) that were compatible
176 with these clusters as explanatory variables. The DFUs were randomly assigned to the
177 training set and the validation set in a 7:3 ratio. The "caret" R package was used to
178 automatically fine-tune model parameters through grid search, default settings. Next,
179 a 5-fold cross-validation was performed for evaluation. The "DALEX" package
180 (version 2.4.2) was employed to explain and visualize the 4 machine learning models.
181 The "pROC" package (version 1.18.0) was used to display the area under the receiver
182 operating characteristic curve (AUC). The top 5 key variables of gene correlation in
183 DFU were depended on the optimal machine learning model.

184 **Developing and independently validating a nomogram model**

185 Using the "rms" R package (version 6.3.0), a nomogram model was developed to
186 assign scores to each predictor variable. The "Total Score" was the cumulative sum of
187 the scores for the predictive variables. Calibration curve and decision curve analysis
188 (DCA) were used to evaluate the predictive performance of the nomogram model. The
189 model to differentiate between DFU and normal samples was independently validated
190 with external datasets GSE134431, GSE68183, and GSE80178.

191 **Interactions between drugs and genes**

192 Advancements in bioinformatics have emphasized the importance of creating
193 biological models and identifying effective biomarkers for disease diagnosis.
194 However, applying these biomarkers in clinical practice was essential. The use of
195 information markers to predict drug response was critical for the prevention and
196 treatment of DFU. The DGIdb database assisted in forecasting drug-gene interactions
197 for key genes identified for the RF model, enhancing drug prediction accuracy and

guiding therapeutic strategies.

Ethical approval and informed consent

There were no clinical trials involved in the study; so, ethical approval and consent of participants were not required.

Results

NRGs expression in DFUs

37 diferentially expressed NRGs (deNRGs) were identifed. Of these, compared with a normal control group, in DFU patients, the expression level of CTPS1, PIPK3, CAMK2A, CAMK2D, PPID, VDAC2, PYGL, PLA2G4A, PLA2G4B, IL1B, CHMP2B, VPS4B, CHMP1B, IL1A, TNFRS10A, IFNA1, STAT5A, STAT5B, and TICAM1 were significantly increased. Conversely, RNF31, CAMK2B, CAMK2G, SLC25A4, SLC25A6, GLUD1, GLUL, PYGB, PLA2G4F, CHMP2A, CHMP3, VPS4A, FAF1, SRAT3, STAT6, TLR3, SQSTM1, HSP90AB1, and BCL2 showed lower expression levels in testicular tissue of patients with DFU (Figure 2A,B). Figure 2C illustrated the chromosomal locations of the NRGs were determined and presented visually in circle forma. Following this, correlation analysis was conducted on the genes (Figure 2D,E), revealing that most exhibited positive interrelationships.

Immune infiltration analysis

Figure 3A depicted the distribution of immune cells in different samples, while Figure 3B highlighted the differences between DFU and normal. In DFU samples, activated Mast cells and Neutrophils were elevated, whereas activated NK cells and CD8 T cells were reduced compared to controls. The correlation between immune cells and NRGs was demonstrated in Figure 3C.

Cluster analysis

When k was set to 2, the highest within-group correlations emerge, suggesting that NRGs can categorize patients with diabetic foot ulcers into two distinct clusters (Figure 4A). Figure 4B highlighted notable variations in the principal component

243 analysis (PCA) across clusters. Further, the NRGs across the various clusters were
244 investigated following this cluster analysis. Significant variations were observed in
245 the levels of RNF31, GLUD1, PYGB, CHMP2A, CHMP2B, VPS4A, CHMP1B,
246 STAT3, STAT5A, HSO90AB1, and PARP1 among groups (Figure 4C,D). Figure 4E
247 and F illustrated the analysis of immune cell infiltration outcomes according to the
248 identified clusters.

249 **Functional enrichment study**

250 Assessing the enrichment of NRGs through GSVA. The pathway was
251 significantly enriched in key genes involved in small cell lung cancer, as well as in the
252 functions of arachidonic acid metabolic pathway genes and metabolites (Figure 5A).
253 The results of the GO analysis showed enzyme substrate adaptation and transportation
254 of compounds containing nucleobases (Figure 5B).

255 **Identification and development of gene modules within co-expression networks**

256 We utilized WGCNA to develop co-expression networks for healthy controls and
257 DFU patients, revealing significant gene modules related to DFU. We discovered gene
258 modules that exhibited co-expression under this specific condition (Figure 6A).
259 Subsequently, the dynamic cut algorithm resulted in 26 unique co-expression
260 components, distinguished with various colors, then created a TOM heat map (Figure
261 6B,C,D). Furthermore, we analyzed the correlation and consistency of co-expression
262 patterns using genes from these 26 modules in relation to clinical characteristics. The
263 red module contained 222 hub genes, had the strongest correlation with DFU (Figure
264 6E) and exhibited a positive association (Figure 6F).

265 Moreoverer, the pivotal gene modules related to NRGs were identified by
266 WGCNA. A scale-free network was constructed with the soft threshold parameter β
267 = 12 and R^2 = 0.9 (Figure 7A). 22 important modules were analyzed, and a heatmap
268 displayed the TOM of genes associated with these modules (Figure B,C,D).
269 Analyzing the relationship of modules and clinical picture illustrated the significance
270 of pink color module (Figure 7E). Figure 7 showed the correlation analysis, revealing
271 the strong positive association of the pink module and hub gene.

272 **Modeling**

273 By aligning these genes of pink color module from NRGs clusters with those of
274 the red module from DFU, we identified 10 unique NRGs (Additional fle 1: Appendix
275 1) specific to these clusters (Figure 8A,B). The analysis of residual distributions
276 across the four models indicated that the RF model has the largest residuals (Figure
277 8B). Figure 8C showed the top 10 important characteristics of models. As shown in
278 Figure 8D, the ROC analysis of the 4 machine models revealed that the RF model
279 achieved a perfect AUC value of 1.000. As a result, the RF model (CENPB, TRIM56,
280 ZNF768, PLIN4, and ATP1A1) (Figure 8E) was selected as the most suitable model
281 because it could most clearly distinguish between DFU and normal samples.

282 **Assessment of machine models**

283 The predictive performance of the RF model was evaluated by line graphs
284 (Figure 9A). The calibration graph showed the closest alignment between the real and
285 predicted risk of DFU clustering (Figure 9B). DCA demonstrated that the line graph
286 was highly accurate and provided valuable insights for clinic treatment (Figure 9C).
287 After validating the model with datasets GSE134431, GSE80178, and GSE68183

288 (Figure 9D), ROC analysis showed perfect discrimination with an AUC of 1.000.
289 Figure 9 showed an immune-correlation analysis of the model genes, highlighting
290 their immune function.

291 **Drug-gene interactions analysis**

292 The interacting genes were utilized for predicting drug interactions. From target
293 ATP1A1, we predicted drugs such as ISTAROXIME, DIGOXIN,
294 ACETYLDIGITOXIN, ARTEMETHER, ALMITRINE, DESLANOSIDE, BEPRIDIL,
295 LUMEFANTRINE, DIGITOXIN, OUABAIN, EPLERENONE, and
296 CHLOROPROCAINE. (Additional file 1: Appendix 2).

297
298
299
300
301
302
303
304
305
306
307
308
309
310
311
312
313
314

315 **Discussions**

316 Diabetes is a persistent metabolic disorder that can only be managed[35], not
317 cured. Complications resulting from long-term poor blood glucose control, including
318 cardiovascular and cerebrovascular diseases, as well as renal failure[36,37]. DFU is a
319 common complication of diabetes among others. While nanodressings, bioactive
320 dressings, and 3D printed dressings have been created for DFU treatment[38], current
321 dressings prioritize therapy over real-time monitoring and wound response. Our
322 understanding of the molecular basis of DFU has significantly increased in the last
323 few decades[39,40]. This highlights the potential of biomarkers for various aspects of
324 treatment, including diagnostics, disease diagnosis, disease prognosis, and new drug
325 research. While the underlying mechanisms contributing to the development of DFU
326 remains uncertain. Hence, we theorize that there is a complex relationship between
327 NRGs and the development of DFU. We used bioinformatics methods in our study to
328 investigate the potential connection between them[41].

329 Necroptosis, as a novel therapeutic target, has received increasing attention, is
330 gaining more recognition and its impact is seen differently in various clinical
331 environments. Necroptosis is a basic physiological phenomenon in human body,
332 involves intricate interactions between necrosis and apoptosis, demonstrating distinct
333 regulatory pathways. The initiation of necroptosis involves the activation of specific
334 cell surface receptors including Toll-like receptors, tumor necrosis factor receptor 1,
335 and interferon receptors. This activation leads to the formation of the necrosome
336 genes, involving crucial molecules such as receptor-interacting protein kinases, which

are essential for orchestrating the necroptotic process[42-44]. Several research studies have connected interrupted necroptosis with brain damage and the onset of cancer, leading to the approval of medications targeting necroptosis for the treatment of different neurological conditions and malignant tumors[45]. Naito et al. found that cerebral ischemia-reperfusion injury can rapidly activate necrotic apoptosis, promote cerebral hemorrhage and neuroinflammation, and aggravate brain injury[46]. Necroptosis in triple-negative breast cancer promotes the formation of vasculogenic mimicry through RIPK1/p-AKT/eIF4E signaling pathway[47]. The exact function of necroptosis in the development of DFU remains unclear, and this could represent a promising feld.

This study unsupervised clustering analysis to explore distinct patterns of necroptosis regulation using the expression profiles of NRGs, identifying two unique clusters of NRGs. Furthermore, this study innovatively constructed machine learning models using disease characteristics and pivotal genes identified through WGCNA within the two unique NRG clusters. As research evolves, there' s a growing trend of using machine learning models for DFU prediction. Unlike the conventional univariate analysis, machine learning typically utilizes a multivariate analysis method, considering the interactions among variables. Hence, machine learning models tend to be more precise and produce more dependable outcomes. The "caret" R package utilized functions as an extensive machine learning toolkit aimed at solving prediction issues. Its main attribute is the rapid setup of essential elements, ultimately completing the model prediction[48]. We evaluated the predictive capabilities of the

359 following models: RF, SVM, XGB, and GLM. The model built using RF
360 demonstrated extremely high accuracy on the test dataset (AUC = 1.000), highlighting
361 a strong predictive level. Furthermore, we developed a bar and line chart model for
362 DFU, employing the following genes: CENPB, TRIM56, ZNF768, PLIN4, and
363 ATP1A1. Our findings indicated that the model demonstrated strong predictive ability,
364 suggesting its viability for clinical use. Overall, the RF model utilizing five genes to
365 identify DFU subtypes proved to be effective.

366 Using the RF algorithm, we detected five key NRGs (CENPB, TRIM56,
367 ZNF768, PLIN4, and ATP1A1) and confirmed their diagnostic capabilities through a
368 separate dataset, suggesting their relevance to the mechanism of DFU. The CENPB
369 gene is a critical protein that operates in the centromeric region of chromosomes,
370 ensuring proper chromosome segregation during cell division[49]. CENPB
371 predominantly attaches to a-satellite DNA at the centromere and participates in the
372 formation of kinetochores, which connect chromosomes to the mitotic spindle during
373 cellular division[50]. CENPB plays a role in controlling various cellular functions,
374 such as gene expression, DNA repair mechanisms, and DNA replication[51]. TRIM56,
375 part of the TRIM protein family, acts as an E3 ubiquitin ligase that is inducible by
376 interferons and can increase expression when stimulated by double-stranded DNA. It
377 modulates the stimulator of interferon genes, facilitating the synthesis of type I
378 interferon and boosting innate immune responses[52]. PLIN4 belongs to the PAT
379 protein family involved in lipid storage droplets and serves as a key regulator of lipid
380 storage[53]. Reduced expression of this protein has been linked to weight gain[54].

381 ATP1A1 causes a range of disorders, impacting the endocrine and neuromuscular
382 systems[55,56], while also disrupting the renal and central nervous systems[57].
383 According to a recent study, elevated ATP1A1 expression correlates with unfavorable
384 long-term outcomes in individuals diagnosed with colon cancer and regulates tumor
385 progression[58]. Unfortunately, there are limited studies on CENPB, TRIM56,
386 ZNF768, PLIN4, and ATP1A1 in DFU.

387 The acute wound healing process comprises four dynamic overlapping and
388 differentiated stages: hemostasis, inflammation, proliferation, and remodeling. This
389 process is subject to many kinds Type cells are strictly controlled and associated with
390 cell migration and proliferation, ECM deposition and group Weave remodeling related.
391 Chronic inflammation is the main culprit of normal wound healing disorder[59].
392 Chronic inflammation impairs wound healing by altering the bactericidal function of
393 immune cells, reducing vascular perfusion, disrupting the basement membrane and
394 collagen synthesis. Hyperglycemia leads to the formation of microthrombus through
395 the production of inflammatory mediators mediated by the increase of reactive
396 oxygen species, pericellular degeneration, basement membrane thickening,
397 endothelial hyperplasia, decreased vasodilation, and increased coagulant promoting
398 markers. Microthromboembolism may be more likely to occur in microvessels, thus
399 aggravating the local tissue ischemia and hypoxia of diabetic wound and nerve
400 damage[60].

401 Research on biomarkers related to DFU remains somewhat scarce. Lately,
402 bioinformatics analysis has emerged as a useful means for investigating the detailed

and multifaceted relationships between cell necrosis, cell apoptosis, and DFU[61,62]. A detailed investigation has revealed potential biomarkers for DFU utilizing transcriptomics and proteomics bioinformatics approaches. It highlighted MMP9, FABP5, and ITGAM as central genes, indicating their potential roles as molecular targets in DFU' s immunotherapy treatments[63]. However, there are only a handful of studies focusing on predictive models related to necroptosis in DFU. By exploring the mechanisms of necroptosis, this study offers valuable insights for the development of effective immunotherapy strategies in DFU. Initially, we gathered extensive data about NRGs from the GEO databases to build on prior study insights. We primarily analyzed GSE134431, supplemented by GSE80178 and GSE68183 to verify the trends observed. The validity of the study was reinforced by GO and KEGG analyses, along with the support of GSVA. Finally, few existing predictive models for NRGs offer targeted suggestions for future immunoinflammatory studies or treatments involving necroptosis interference in DFU. The study employed machine learning techniques to develop a diagnostic framework for necroptosis and DFU, integrating immune cell infiltration analysis. The computational outcomes highlighted the connections between necroptosis, DFU, and the immune responses, broadening the approach to linking gene expression with clinical practice. Moreover, continued advances in artificial intelligence provides essential ideas for medical professionals and promises to enhance our understanding of DFU and future therapeutic strategies.

Translation

Certainly, our model is not without its limitations. First of all, depending on data from the GEO database introduces difficulties in evaluating the statistical data' s quality and reliability. To mitigate this, GSE134431 was selected as the primary dataset, and model validation was conducted using GSE13443, GSE80178, and GSE68183 due to their well-defined grouping. Secondly, the sample size of this study was not sufficiently large, which may have impacted the robustness of the findings. Future studies with a larger sample size are planned to further validate these results. Thirdly, a significant challenge lies in the limited analysis of genes associated with NRGs and DFU, resulting in a lack of knowledge regarding the underlying mechanisms. Future research should include foundational experiments to enhance validation. Lastly, further exploration of parameter selection within the model, combined with experimental studies, is required to identify the final genes.

Conclusions

Necroptosis plays a role in the synthesis of CENPB, TRIM56, ZNF768, PLIN4, and ATP1A1, leading to the construction of a diagnostic model. Future enhancements include expanding data sources and undertaking further research to explore the potential of effective treatments in reducing inflammation in DFUs by targeting necroptosis pathways. Our findings present promising biomarkers for the development of DFU treatment strategies. This study have examined the possibility of using NRGs as biomarkers for DFU in order to advance treatment of this condition.

Funding

We thank the databases mentioned in our study. This study was supported by the National Natural Science Foundation of China (82274528).

Competing interests

The authors declare no competing interests.

References

1. Zhang Y, Lazzarini P A, Mcphail S M, et al. Global Disability Burdens of Diabetes-Related Lower-Extremity Complications in 1990 and 2016[J]. Diabetes Care,2020,43(5):964-974.
2. Davies A H. The Seriousness of Chronic Venous Disease: A Review of Real-World Evidence[J]. Advances in Therapy,2019,36(S1):5-12.
3. Mcdermott K, Fang M, Boulton A J M, et al. Etiology, Epidemiology, and Disparities in the Burden of Diabetic Foot Ulcers[J]. Diabetes care,2023,46(1):209-221.
4. Armstrong D G, Tan T, Boulton A J M, et al. Diabetic Foot Ulcers[J]. JAMA,2023,330(1):62.
5. Shofler D, Rai V, Mansager S, et al. Impact of resolvin mediators in the immunopathology of diabetes and wound healing[J]. Expert Rev Clin Immunol,2021,17(6):681-690.
6. Sun H, Pulakat L, Anderson D W. Challenges and New Therapeutic Approaches in the Management of Chronic Wounds[J]. Curr Drug Targets,2020,21(12):1264-1275.
7. Cano Sanchez M, Lancel S, Boulanger E, et al. Targeting Oxidative Stress and Mitochondrial Dysfunction in the Treatment of Impaired Wound Healing: A Systematic Review[J]. Antioxidants,2018,7(8):98.
8. Patel S, Srivastava S, Singh M R, et al. Mechanistic insight into diabetic wounds: Pathogenesis, molecular targets and treatment strategies to pace wound healing[J]. Biomedicine & Pharmacotherapy,2019,112:108615.
9. Grennan D. Diabetic Foot Ulcers[J]. JAMA,2019,321(1):114.
10. Kang Y, Zheng C, Ye J, et al. Effects of advanced glycation end products on neutrophil migration and aggregation in diabetic wounds[J]. Aging (Albany NY),2021,13(8):12143-12159.
11. Liao S, Apaijai N, Chattipakorn N, et al. The possible roles of necroptosis during cerebral ischemia and ischemia / reperfusion injury[J]. Archives of Biochemistry and Biophysics,2020,695:108629.
12. Balusu S, Horre K, Thrupp N, et al. MEG3 activates necroptosis in human neuron xenografts modeling Alzheimer's disease[J]. Science,2023,381(6663):1176-1182.
13. Vucur M, Ghallab A, Schneider A T, et al. Sublethal necroptosis signaling promotes inflammation and liver cancer[J]. Immunity,2023,56(7):1578-1595.
14. Li F, Sun H, Yu Y, et al. RIPK1-dependent necroptosis promotes vasculogenic mimicry formation via eIF4E in triple-negative breast cancer[J]. Cell Death Dis,2023,14(5):335.
15. Li Z, Dai R, Chen M, et al. p55gamma degrades RIP3 via MG53 to suppress ischaemia-induced myocardial necroptosis and mediates cardioprotection of preconditioning[J]. Cardiovasc Res,2023,119(14):2421-2440.
16. Wu X, Nagy L E, Gautheron J. Mediators of necroptosis: from cell death to metabolic regulation[J]. EMBO Mol Med,2024,16(2):219-237.
17. Zhong B, Wang Y, Liao Y, et al. MLKL and other necroptosis-related genes promote the tumor immune cell infiltration, guiding for the administration of immunotherapy in bladder urothelial carcinoma[J]. Apoptosis,2023,28(5-6):892-911.
18. Zhang T, Xu D, Liu J, et al. Prolonged hypoxia alleviates prolyl hydroxylation-mediated suppression of RIPK1 to promote necroptosis and inflammation[J]. Nat Cell Biol,2023,25(7):950-962.
19. Zou J, Zhang W, Chen X, et al. Data mining reveal the association between diabetic foot ulcer and peripheral artery disease[J]. Front Public Health,2022,10:963426.
20. Wang X, Meng L, Zhang J, et al. Identification of ferroptosis-related molecular clusters and genes for diabetic osteoporosis based on the machine learning[J]. Front Endocrinol

(Lausanne),2023,14:1189513.
21. Yang L, Li L P, Yi H C. DeepWalk based method to predict lncRNA-miRNA associations via lncRNA-miRNA-disease-protein-drug graph[J]. BMC Bioinformatics,2022,22(Suppl 12):621.
22. Sheng N, Wang Y, Huang L, et al. Multi-task prediction-based graph contrastive learning for inferring the relationship among lncRNAs, miRNAs and diseases[J]. Brief Bioinform,2023,24(5):bbad276.
23. Li J, Wang H, Dong C, et al. The underlying mechanisms of FGF2 in carotid atherosclerotic plaque development revealed by bioinformatics analysis. Arch Med Sci 2024;20:1209-19.
24. Sun F, Sun J, Zhao Q. A deep learning method for predicting metabolite-disease associations via graph neural network[J]. Brief Bioinform,2022,23(4):bbac266.
25. Gao H, Sun J, Wang Y, et al. Predicting metabolite-disease associations based on auto-encoder and non-negative matrix factorization[J]. Brief Bioinform,2023,24(5):bbad259.
26. Wu Z, Gao Y, Cao L, et al. Purine metabolism-related genes and immunization in thyroid eye disease were validated using bioinformatics and machine learning[J]. Sci Rep,2023,13(1):18391.
27. Chen Z, Zhang L, Sun J, et al. DCAMCP: A deep learning model based on capsule network and attention mechanism for molecular carcinogenicity prediction[J]. J Cell Mol Med,2023,27(20):3117-3126.
28. Hu H, Feng Z, Lin H, et al. Gene function and cell surface protein association analysis based on single-cell multiomics data[J]. Comput Biol Med,2023,157:106733.
29. Ramirez H A, Pastar I, Jozic I, et al. Staphylococcus aureus Triggers Induction of miR-15B-5P to Diminish DNA Repair and Deregulate Inflammatory Response in Diabetic Foot Ulcers[J]. J Invest Dermatol,2018,138(5):1187-1196.
30. Sawaya A P, Stone R C, Brooks S R, et al. Deregulated immune cell recruitment orchestrated by FOXM1 impairs human diabetic wound healing[J]. Nat Commun,2020,11(1):4678.
31. Zhabotynsky V, Inoue K, Magnuson T, et al. A statistical method for joint estimation of cis-eQTLs and parent-of-origin effects under family trio design[J]. Biometrics,2019,75(3):864-874.
32. Wu Z, Zhu M, Kang Y, et al. Do we need different machine learning algorithms for QSAR modeling? A comprehensive assessment of 16 machine learning algorithms on 14 QSAR data sets[J]. Brief Bioinform,2021,22(4):bbaa321.
33. Krause L, Mchardy A C, Nattkemper T W, et al. GISMO--gene identification using a support vector machine for ORF classification[J]. Nucleic Acids Res,2007,35(2):540-549.
34. Rigatti S J. Random Forest[J]. J Insur Med,2017,47(1):31-39.
35. Pinheiro-Machado E, Gurgul-Convey E, Marzec MT. Immunometabolism in type 2 diabetes mellitus: tissue-specific interactions. Arch Med Sci 2023;19:895-911.
36. Polk C, Sampson M M, Roshdy D, et al. Skin and Soft Tissue Infections in Patients with Diabetes Mellitus[J]. Infect Dis Clin North Am,2021,35(1):183-197.
37. Fitridge R, Pena G, Mills J L. The patient presenting with chronic limb-threatening ischaemia. Does diabetes influence presentation, limb outcomes and survival?[J]. Diabetes Metab Res Rev,2020,36 Suppl 1:e3242.
38. Fitridge R, Pena G, Mills J L. The patient presenting with chronic limb-threatening ischaemia. Does diabetes influence presentation, limb outcomes and survival?[J]. Diabetes Metab Res Rev,2020,36 Suppl 1:e3242.
39. Gan Y, Huang X, Zou G, et al. Deep structural clustering for single-cell RNA-seq data jointly through autoencoder and graph neural network[J]. Brief Bioinform,2022,23(2):bbac018.

584 40. Wang T, Sun J, Zhao Q. Investigating cardiotoxicity related with hERG channel blockers using
585 molecular fingerprints and graph attention mechanism[J]. Comput Biol Med,2023,153:106464.
586 41. Shi H, Yuan X, Yang X, et al. A novel diabetic foot ulcer diagnostic model: identification and
587 analysis of genes related to glutamine metabolism and immune infiltration[J]. BMC
588 Genomics,2024,25(1):125.
589 42. Guo B, Chen J H, Zhang J H, et al. Pattern-recognition receptors in endometriosis: A narrative
590 review[J]. Front Immunol,2023,14:1161606.
591 43. Ying L, Benjanuwattra J, Chattipakorn S C, et al. The role of RIPK3-regulated cell death pathways
592 and necroptosis in the pathogenesis of cardiac ischaemia-reperfusion injury[J]. Acta Physiol
593 (Oxf),2021,231(2):e13541.
594 44. Siegmund D, Zaitseva O, Wajant H. Fn14 and TNFR2 as regulators of cytotoxic TNFR1 signaling[J].
595 Front Cell Dev Biol,2023,11:1267837.
596 45. Zhou Y, Cai Z, Zhai Y, et al. Necroptosis inhibitors: mechanisms of action and therapeutic
597 potential[J]. Apoptosis,2024,29(1-2):22-44.
598 46. Naito M G, Xu D, Amin P, et al. Sequential activation of necroptosis and apoptosis cooperates to
599 mediate vascular and neural pathology in stroke[J]. Proc Natl Acad Sci U S A,2020,117(9):4959-4970.
600 47. Li F, Sun H, Yu Y, et al. RIPK1-dependent necroptosis promotes vasculogenic mimicry formation via
601 eIF4E in triple-negative breast cancer[J]. Cell Death Dis,2023,14(5):335.
602 48. Lee J Y, Won D, Lee K. Machine learning-based identification and related features of depression in
603 patients with diabetes mellitus based on the Korea National Health and Nutrition Examination Survey:
604 A cross-sectional study[J]. PLoS One,2023,18(7):e288648.
605 49. Gamba R, Fachinetti D. From evolution to function: Two sides of the same CENP-B coin?[J]. Exp
606 Cell Res,2020,390(2):111959.
607 50. Ohzeki J I, Otake K, Masumoto H. Human artificial chromosome: Chromatin assembly mechanisms
608 and CENP-B[J]. Exp Cell Res,2020,389(2):111900.
609 51. Mohibi S, Srivastava S, Wang-France J, et al. Alteration/Deficiency in Activation 3 (ADA3) Protein,
610 a Cell Cycle Regulator, Associates with the Centromere through CENP-B and Regulates Chromosome
611 Segregation[J]. J Biol Chem,2015,290(47):28299-28310.
612 52. Wang B, Wang Z, Li Y, et al. TRIM56: a promising prognostic immune biomarker for glioma
613 revealed by pan-cancer and single-cell analysis[J]. Front Immunol,2024,15:1327898.
614 53. Crawley S W, Weck M L, Grega-Larson N E, et al. ANKS4B Is Essential for Intermicrovillar
615 Adhesion Complex Formation[J]. Dev Cell,2016,36(2):190-200.
616 54. Low B, Lim C S, Ding S, et al. Decreased GLUT2 and glucose uptake contribute to insulin secretion
617 defects in MODY3/HNF1A hiPSC-derived mutant beta cells[J]. Nat Commun,2021,12(1):3133.
618 55. Schlingmann K P, Bandulik S, Mammen C, et al. Germline De Novo Mutations in ATP1A1 Cause
619 Renal Hypomagnesemia, Refractory Seizures, and Intellectual Disability[J]. Am J Hum
620 Genet,2018,103(5):808-816.
621 56. Ygberg S, Akkuratov E E, Howard R J, et al. A missense mutation converts the Na(+),K(+)-ATPase
622 into an ion channel and causes therapy-resistant epilepsy[J]. J Biol Chem,2021,297(6):101355.
623 57. Lee J S, Lee B I, Park C B. Photo-induced inhibition of Alzheimer's beta-amyloid aggregation in
624 vitro by rose bengal[J]. Biomaterials,2015,38:43-49.
625 58. Sumiyoshi S, Shiozaki A, Kosuga T, et al. Functional Analysis and Clinical Importance of ATP1A1
626 in Colon Cancer[J]. Ann Surg Oncol,2023,30(11):6898-6910.
627 59. Louiselle A E, Niemiec S M, Zgheib C, et al. Macrophage polarization and diabetic wound healing[J].

Transl Res,2021,236:109-116.
60. Kaltsas A. Oxidative Stress and Male Infertility: The Protective Role of Antioxidants[J]. Medicina (Kaunas),2023,59(10):1769.
61. Lee Y S, Kang S U, Lee M H, et al. GnRH impairs diabetic wound healing through enhanced NETosis[J]. Cell Mol Immunol,2020,17(8):856-864.
62. Liu Y, Zhang X, Yang L, et al. Proteomics and transcriptomics explore the effect of mixture of herbal extract on diabetic wound healing process[J]. Phytomedicine,2023,116:154892.
63. Wang Y, Pi Y, Hu L, et al. Proteomic analysis of foot ulcer tissue reveals novel potential therapeutic targets of wound healing in diabetic foot ulcers[J]. Comput Biol Med,2023,159:106858.

Figure Legends:

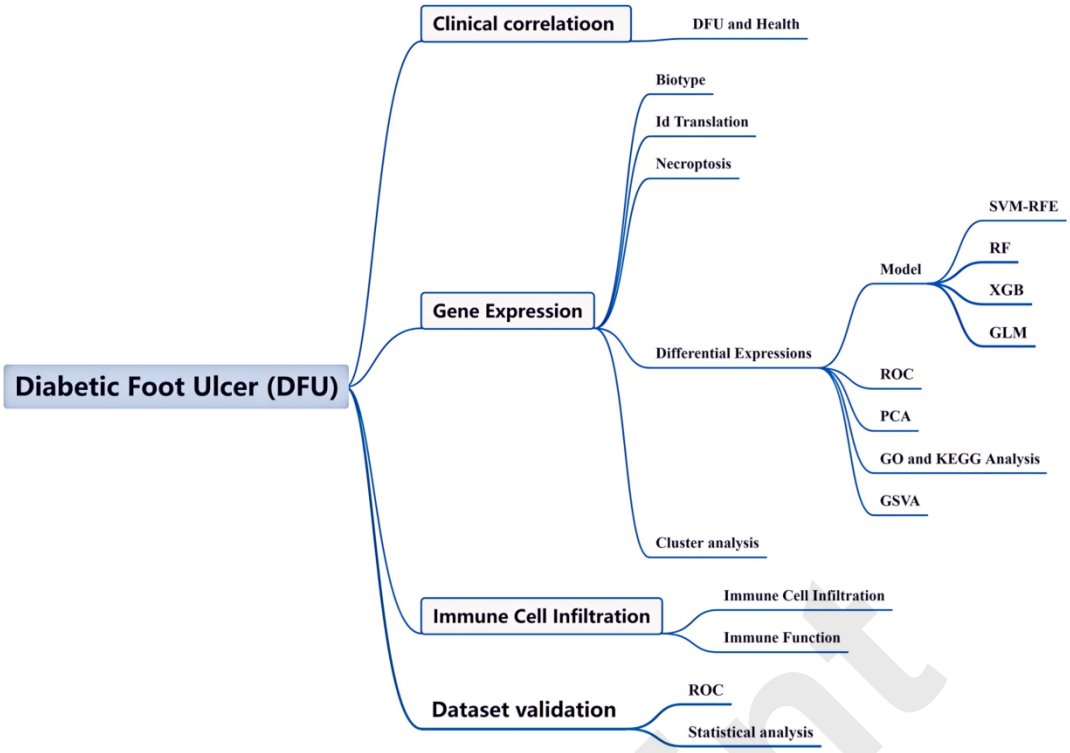

FIGURE 1: Flow chart of this study.

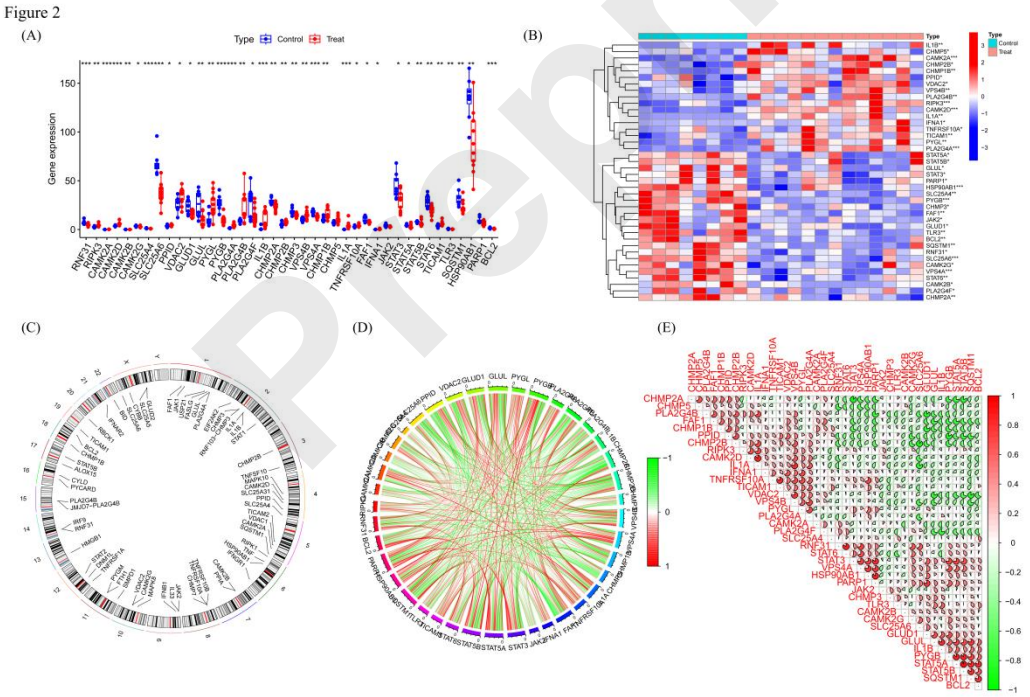

FIGURE 2: Identification of NRGs in DFU. (A) The expression levels of NRGs. (B) Heatmap of NRGs. (C) The location of NRGs on chromosomes. (D) Gene relationship network diagram of NRGs. (E) Correlation analysis of NRGs. Red and green colors represent positive and negative correlations, respectively. The correlation

677 coefficient was expressed as the area of the pie chart.

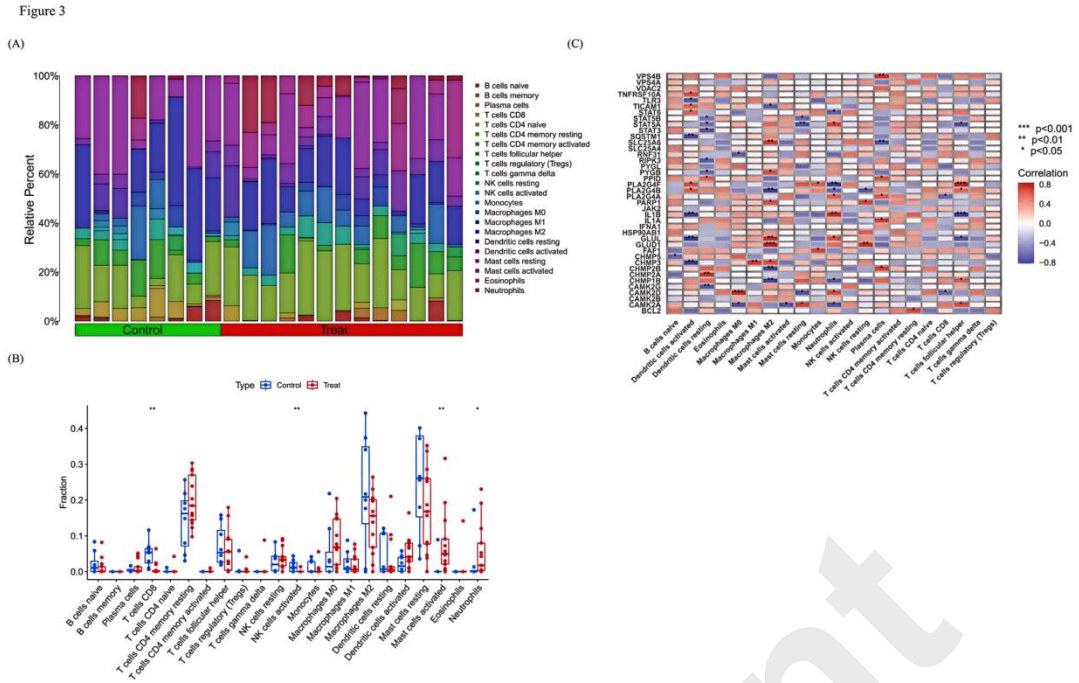

678

679 **FIGURE 3:** Expression of Immune cells. (A) and (B) Expression of immune cells in

680 different clusters. (C) Correlation between NRGs and immune cells.

681

Figure 4

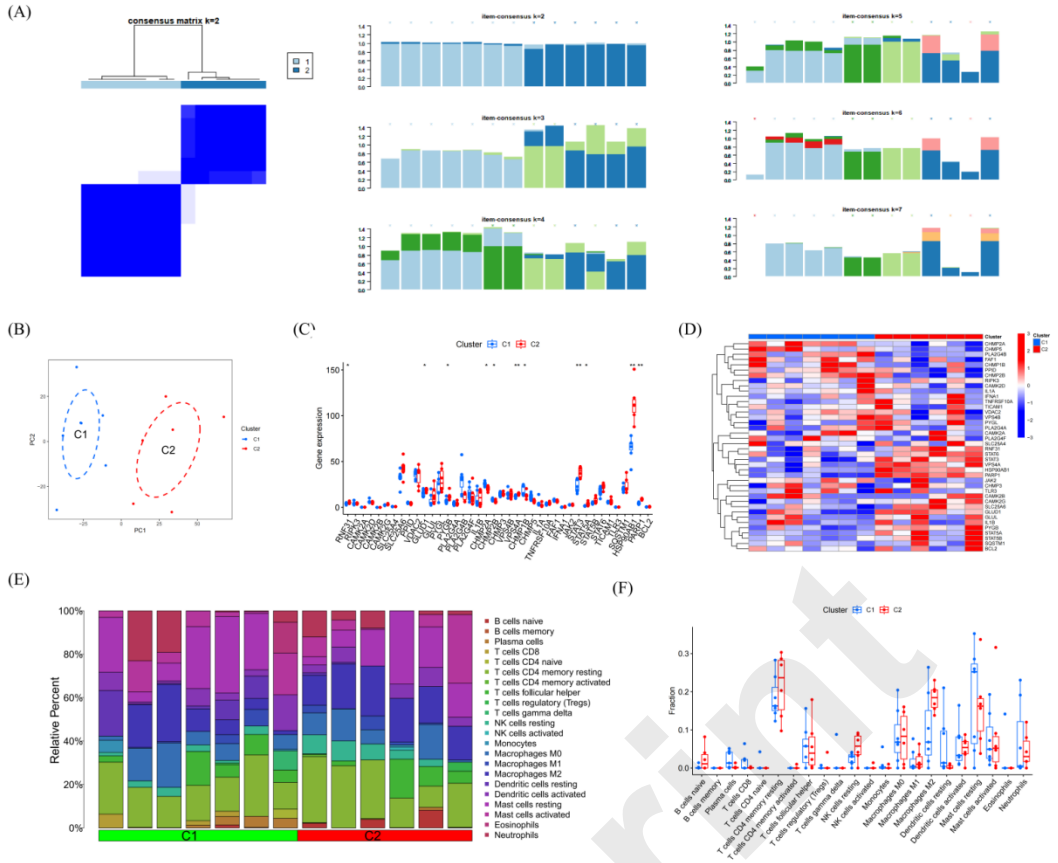

FIGURE 4: Identification of NRGs clusters in DFU. (A) Consensus clustering matrix when k = 2. (B) PCA visualized the distribution of the two clusters. (C) Boxplots of NRGs expressed between the two clusters. (D) Heatmap of the expression patterns of the NRGs between the two clusters. (E) Relative abundance maps of 22 infiltrating immune cells between the two clusters. (F) Boxplots of immune infiltration differences between the two clusters.

Figure 5

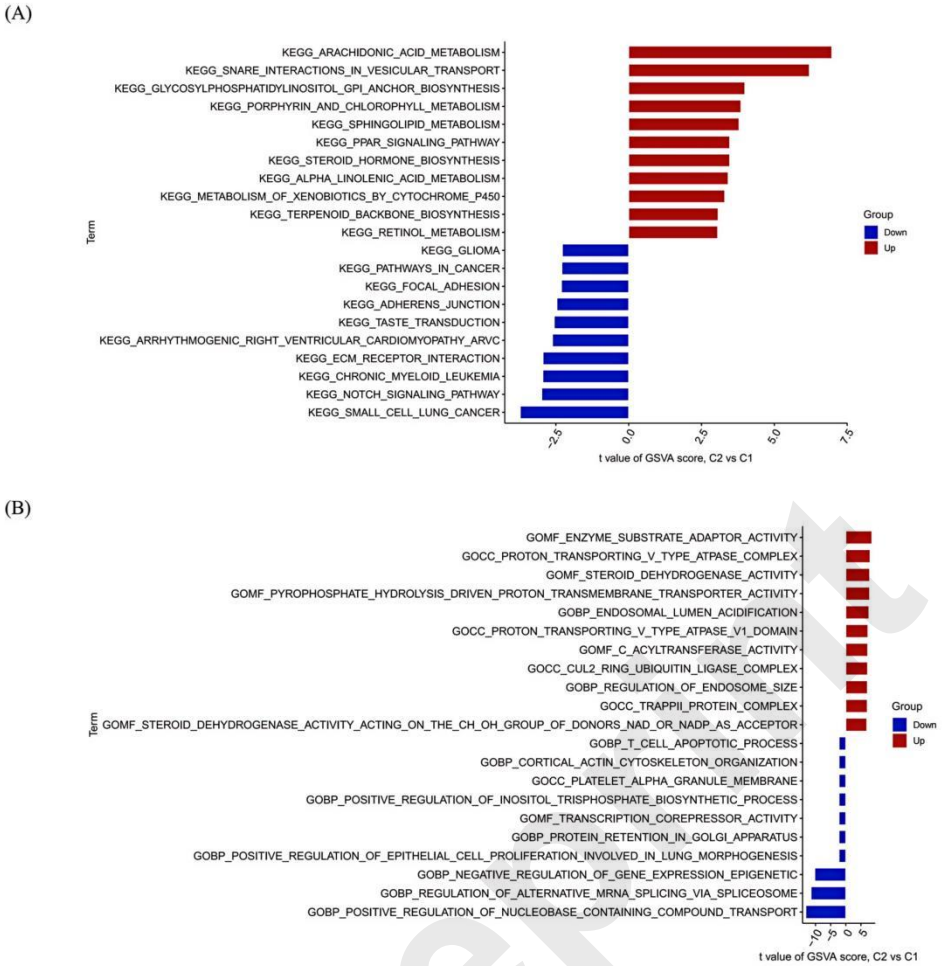

FIGURE 5: Enrichment analysis for NRGs. (A) KEGG. (B) GO.

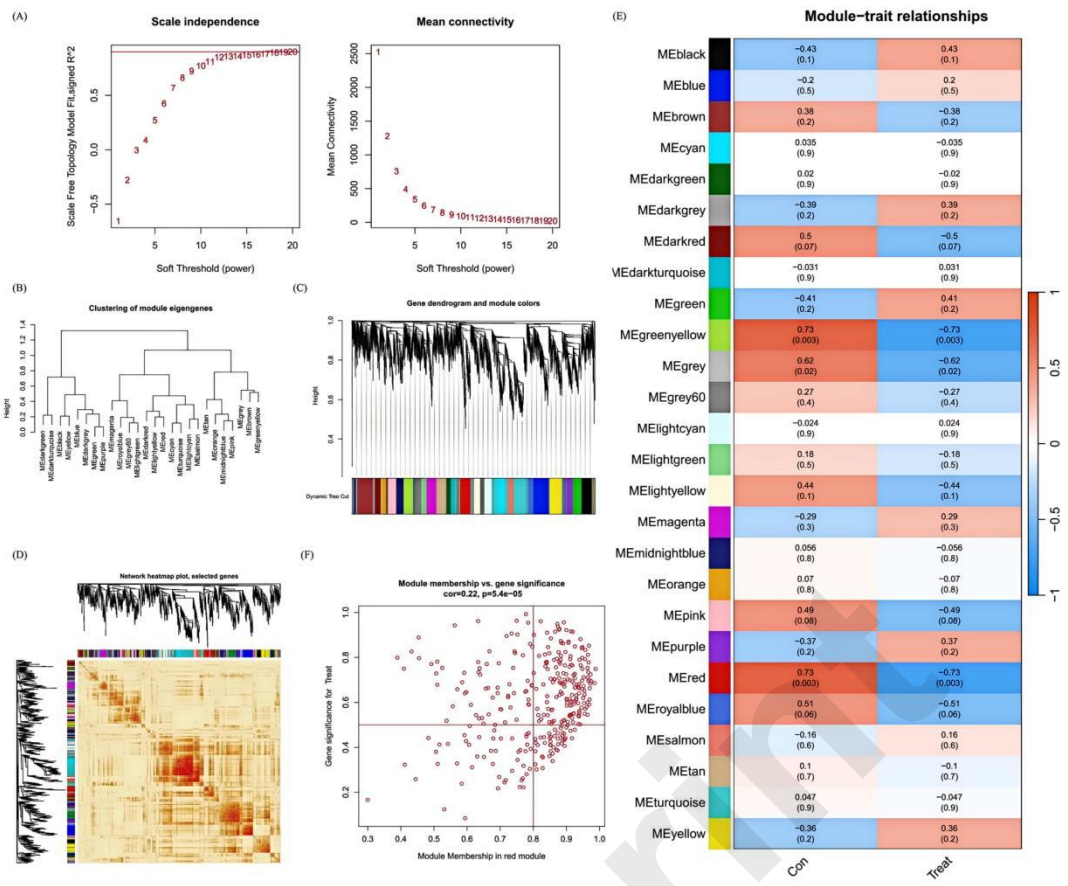

FIGURE 6: Co-expression network of NRGs in DFU. (A) Set soft threshold power. (B) The cluster tree dendrogram of co-expression modules is shown in different colors. (C) Cluster diagram of module eigengenes. (D) TOM heatmap of 26 modules. (E) Heatmap of correlation analysis of module eigengenes with clinical features. Rows and columns represent modules and clinical features, respectively. (F) Scatter plot of the genetic significance of the blue module members with DFU.

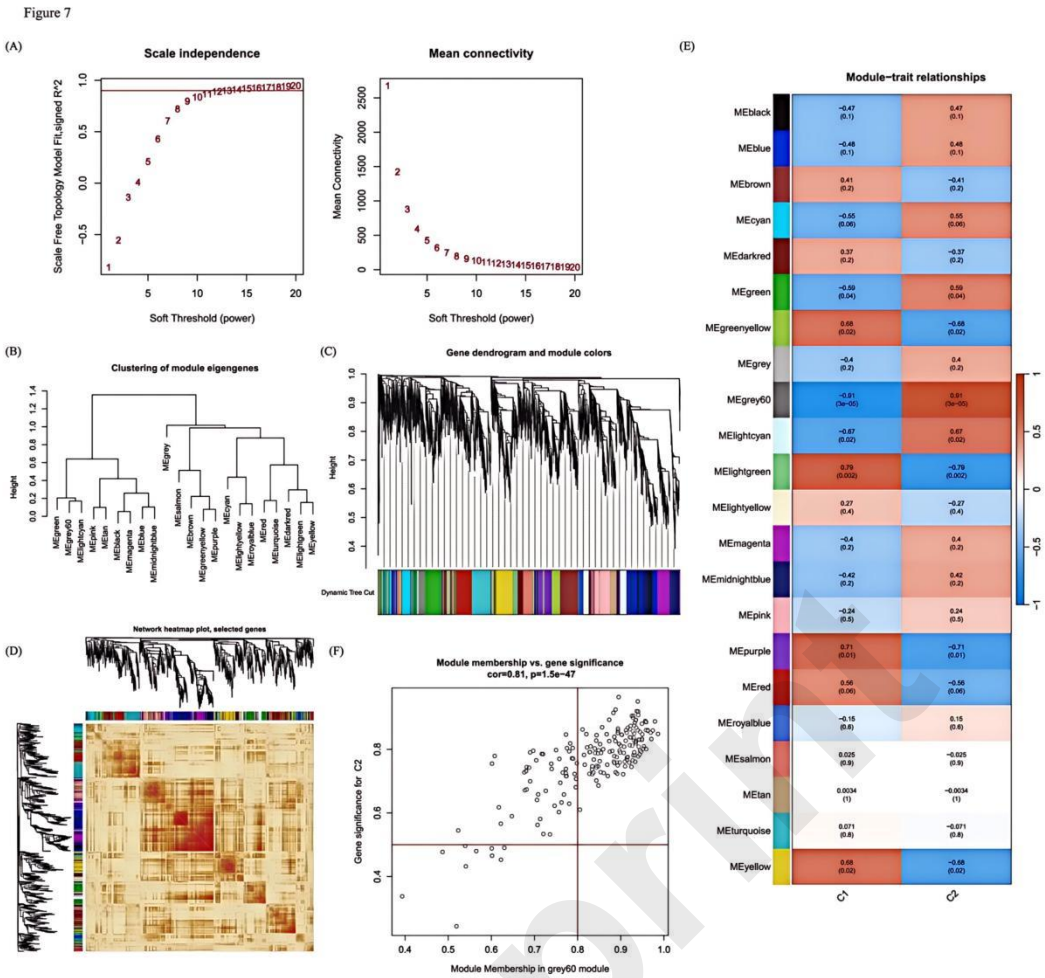

FIGURE 7: Co-expression network of DEGs between the two cuproptosis clusters. (A) Set soft threshold power. (B) The cluster tree dendrogram of co-expression modules is shown in different colors. (C) Cluster diagram of module eigengenes. (D) TOM heatmap of 22 modules. (E) Heatmap of correlation analysis of module eigengenes with clinical features. Rows and columns represent modules and clinical features, respectively. (F) Scatter plot of the genetic significance of the turquoise module members with Cluster1.

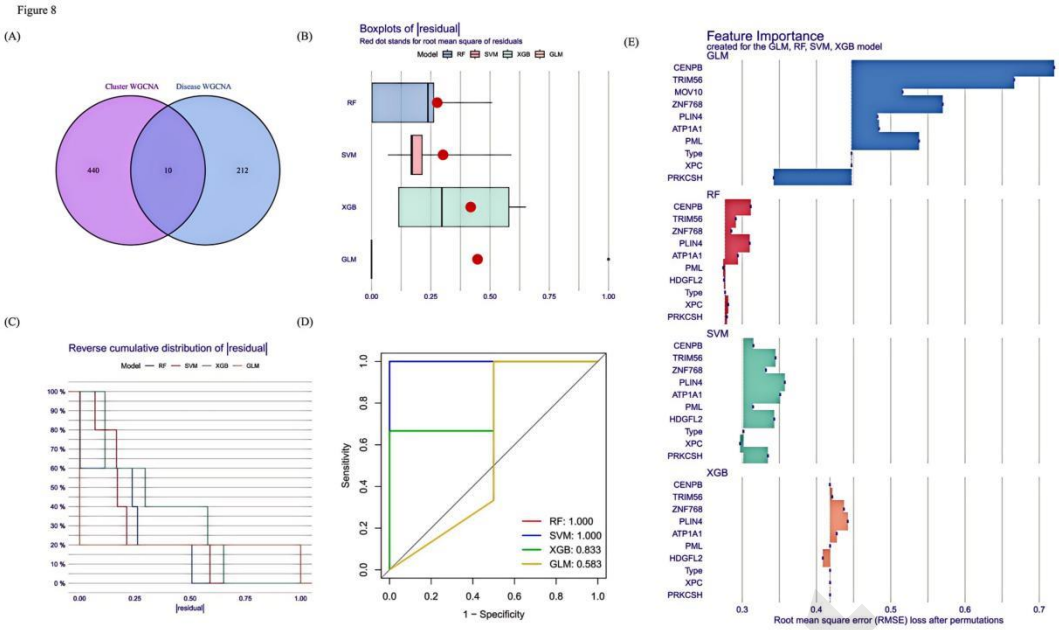

FIGURE 8: Construction of RF, SVM, XGB, and necroptosis models. (A) Crossover genes of the cuproptosis clusters module and the DFU module. (B) The cumulative residual distribution of the four models. (C) Residual Boxplots of the four machine learning models, where the red dots indicate the root mean square of the residuals. (D) ROC analysis of four machine learning models with 5-fold cross-validation in the test set. (E) The important features in RF, SVM, XGB, and GLM.

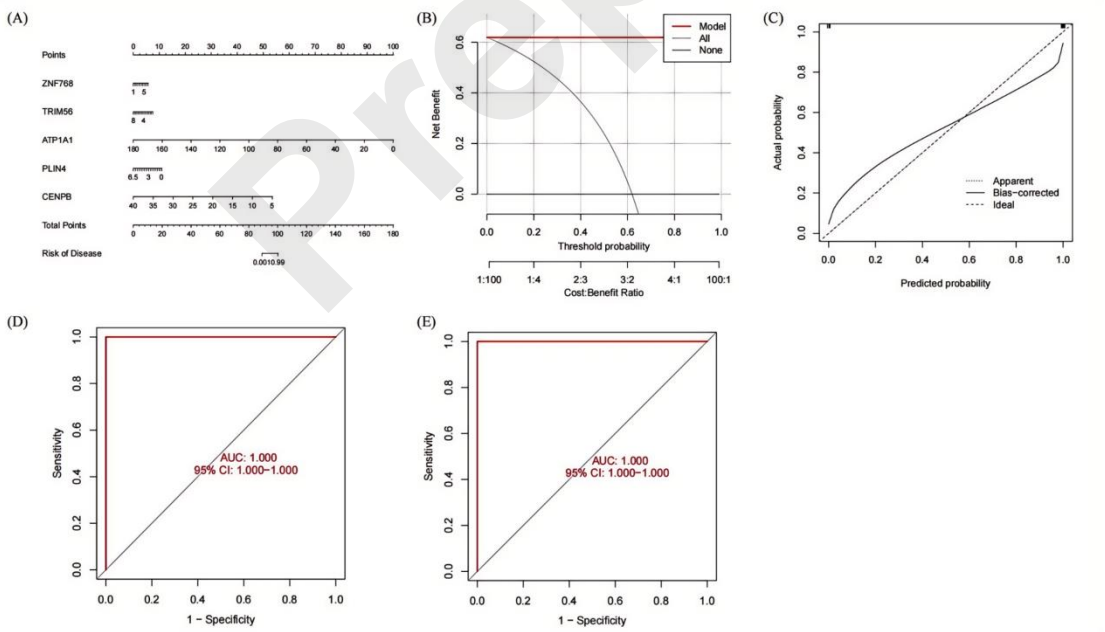

FIGURE 9: Validation of a 5-gene-based RF model. (A) Construction of a nomogram to predict DFU risk based on a 5-gene RF model (B, C) Calibration curves. (D) ROC of the 5-gene-based SVM model (GSE80178). (E) ROC of the 5-gene-based SVM

model (GSE68183).

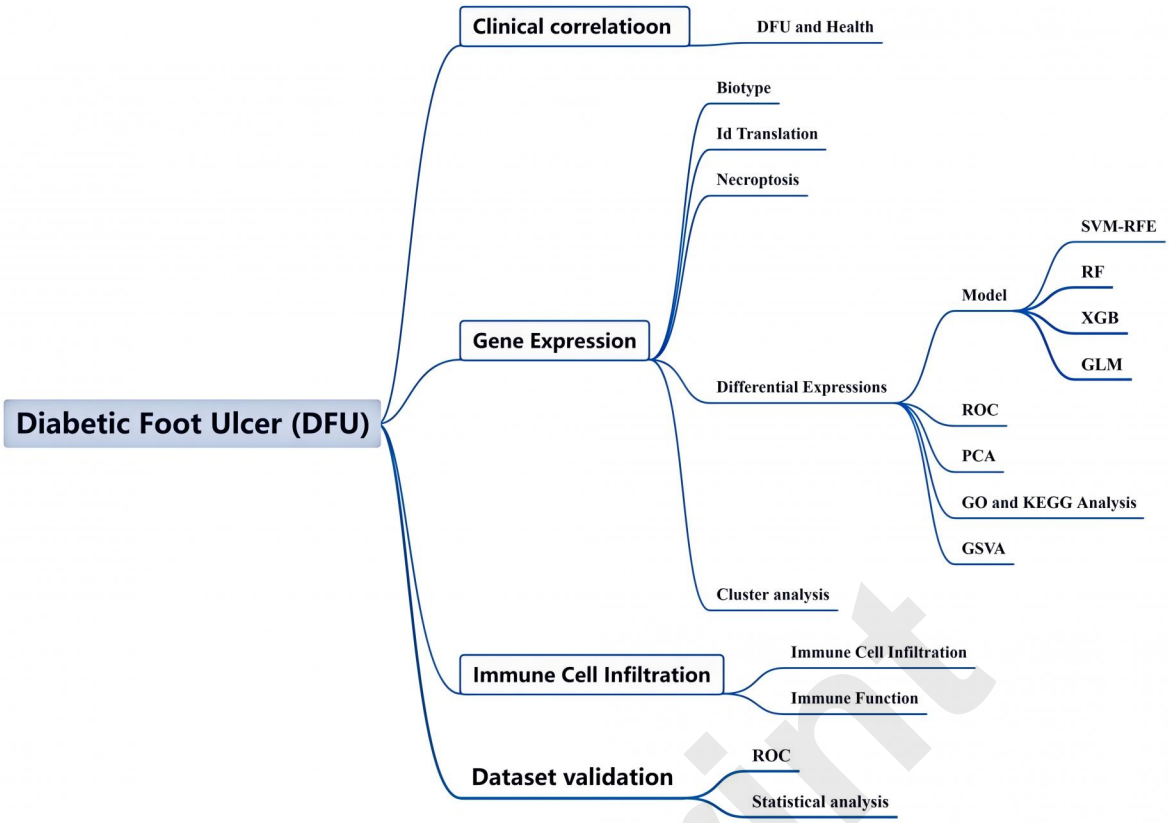
Diabetic Foot Ulcer (DFU)
Clinical correlatioon
DFU and Health
Gene Expression
Biotype
Id Translation
Necroptosis
Differential Expressions
Model
SVM-RFE
RF
XGB
GLM
ROC
PCA
GO and KEGG Analysis
GSVA
Cluster analysis
Immune Cell Infiltration
Immune Cell Infiltration
Immune Function
Dataset validation
ROC
Statistical analysis

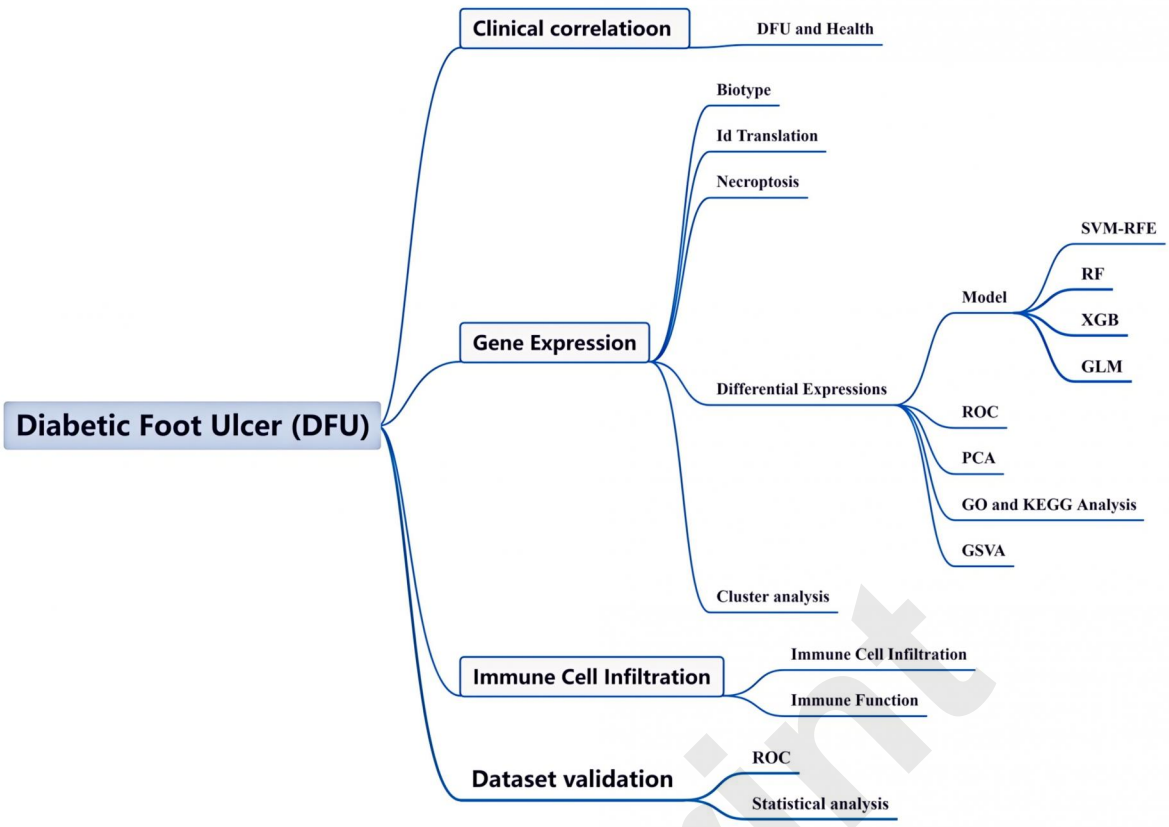
Diabetic Foot Ulcer (DFU)
Clinical correlatioon
DFU and Health
Gene Expression
Biotype
Id Translation
Necroptosis
Differential Expressions
Model
SVM-RFE
RF
XGB
GLM
ROC
PCA
GO and KEGG Analysis
GSVA
Cluster analysis
Immune Cell Infiltration
Immune Cell Infiltration
Immune Function
Dataset validation
ROC
Statistical analysis

Figure 2

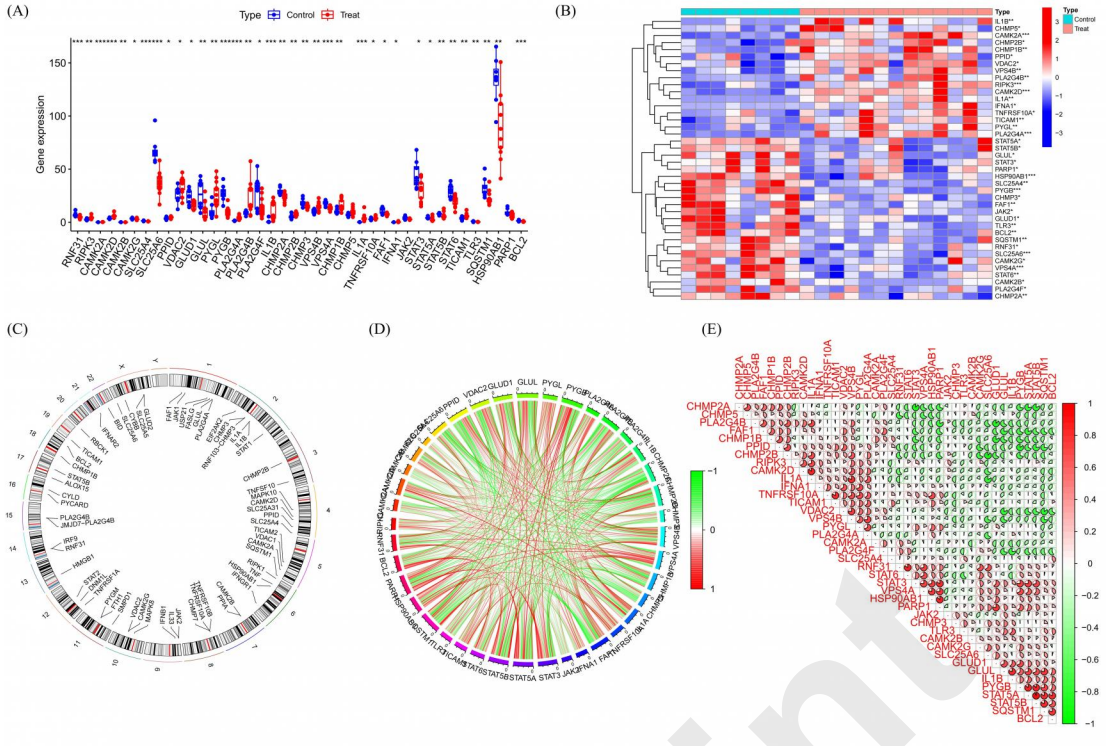

Figure 3

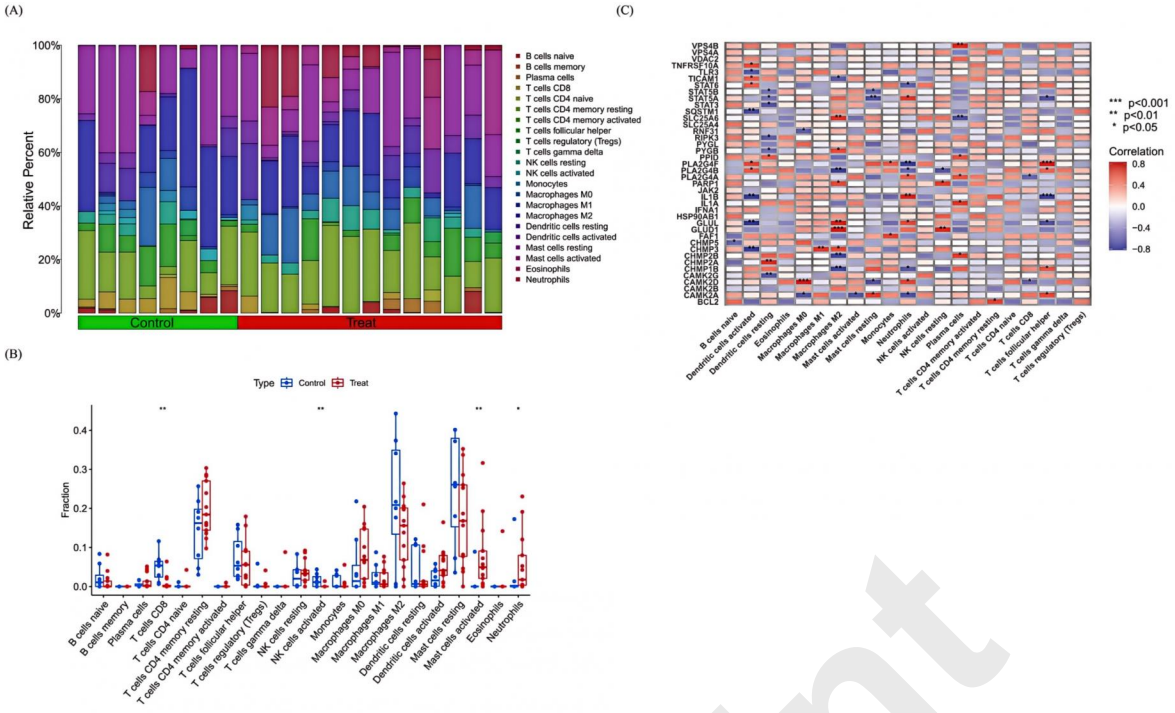

Figure 4

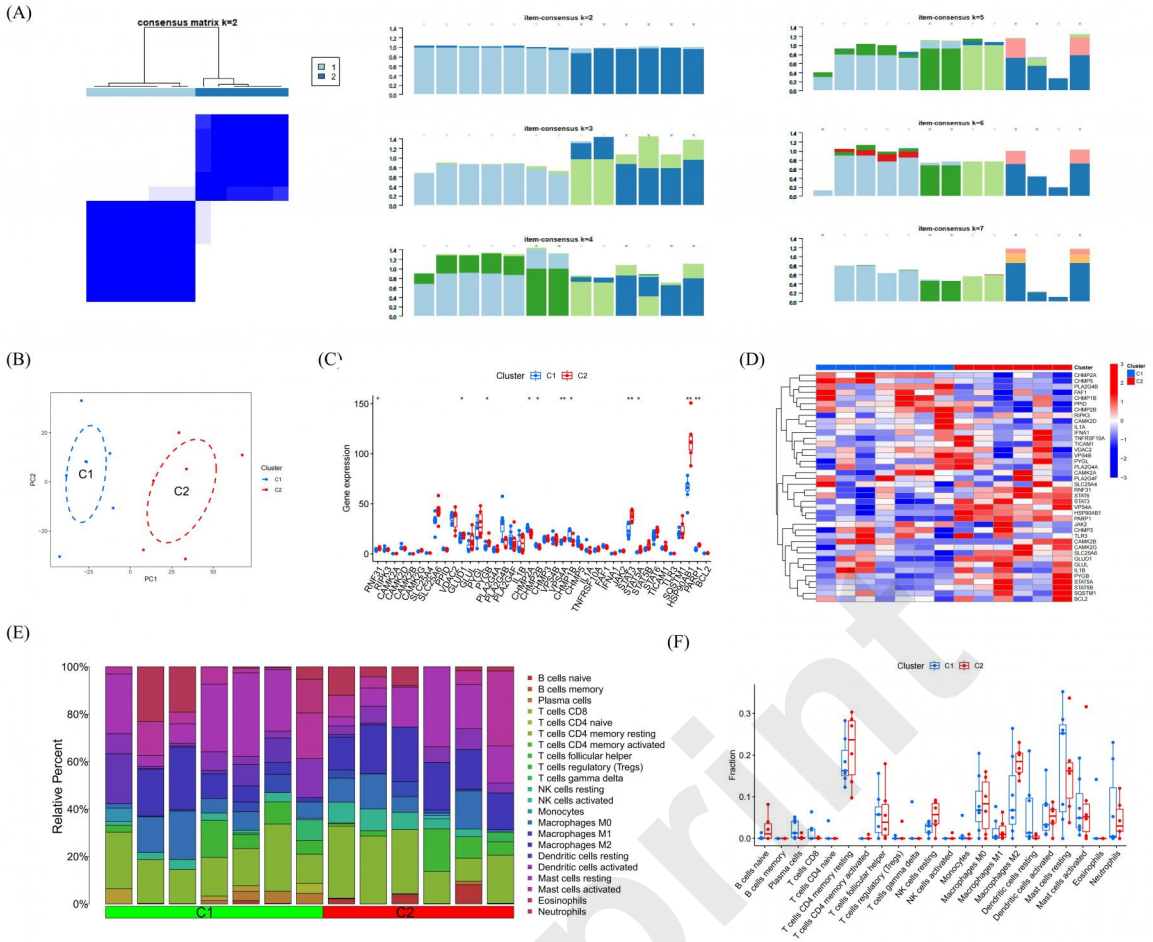

Figure 5

(A)

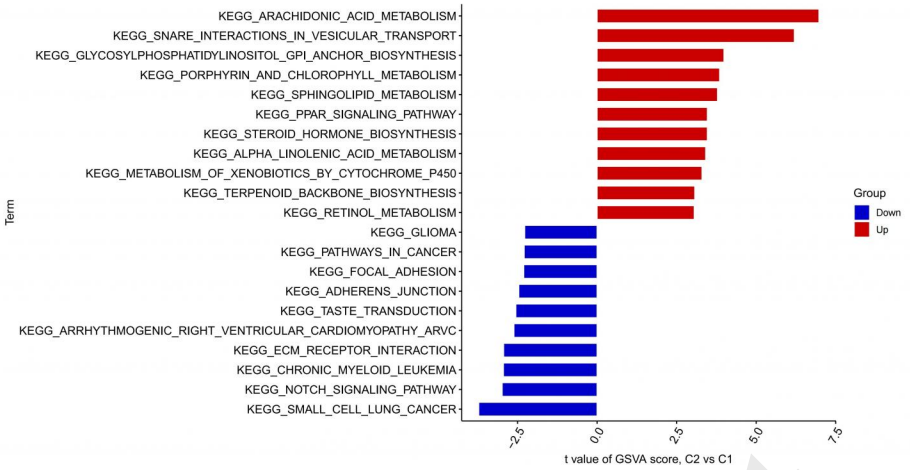

(B)

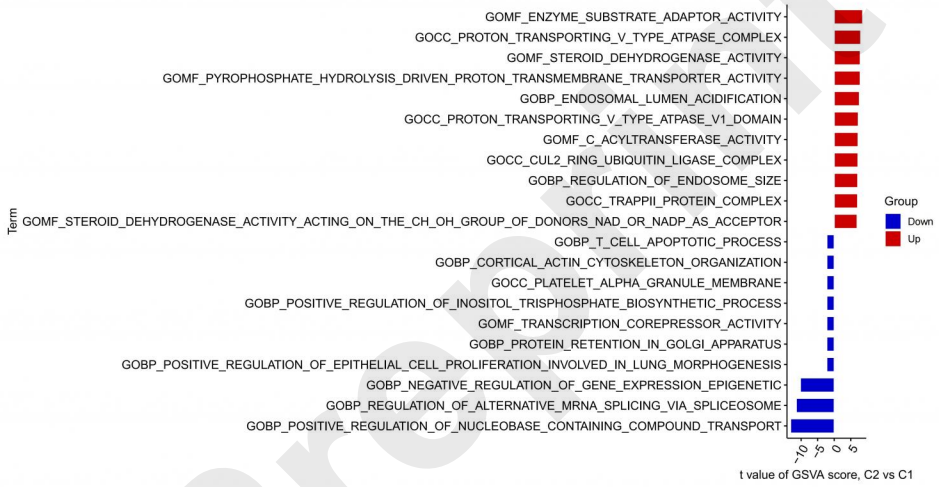

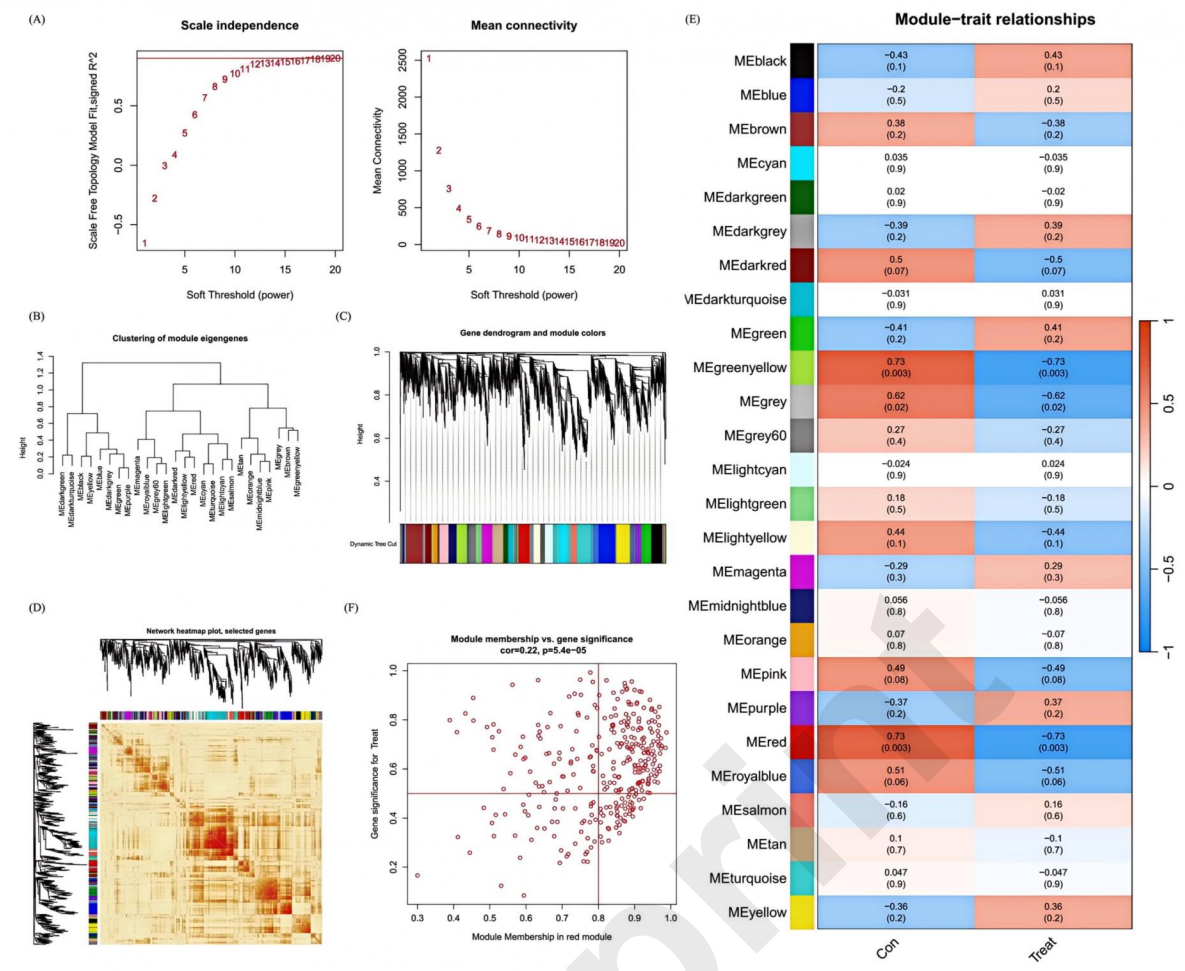
(A)
Scale independence
Scale Free Topology Model Fit,signed R^2
Soft Threshold (power)
Mean connectivity
Mean Connectivity
Soft Threshold (power)
(B)
Clustering of module eigengenes
Height
(C)
Gene dendrogram and module colors
Height
Dynamic Tree Cut
(D)
Network heatmap plot, selected genes
(F)
Module membership vs. gene significance
cor=0.22, p=5.4e−05
Gene significance for Treat
Module Membership in red module
(E)
Module−trait relationships
MEblack −0.43 (0.1) 0.43 (0.1)
MEblue −0.2 (0.5) 0.2 (0.5)
MEbrown 0.38 (0.2) −0.38 (0.2)
MEcyan 0.035 (0.9) −0.035 (0.9)
MEdarkgreen 0.02 (0.9) −0.02 (0.9)
MEdarkgrey −0.39 (0.2) 0.39 (0.2)
MEdarkred 0.5 (0.07) −0.5 (0.07)
MEdarkturquoise −0.031 (0.9) 0.031 (0.9)
MEgreen −0.41 (0.2) 0.41 (0.2)
MEgreenyellow 0.73 (0.003) −0.73 (0.003)
MEgrey 0.62 (0.02) −0.62 (0.02)
MEgrey60 0.27 (0.4) −0.27 (0.4)
MElightcyan −0.024 (0.9) 0.024 (0.9)
MElightgreen 0.18 (0.5) −0.18 (0.5)
MElightyellow 0.44 (0.1) −0.44 (0.1)
MEmagenta −0.29 (0.3) 0.29 (0.3)
MEmidnightblue 0.056 (0.8) −0.056 (0.8)
MEorange 0.07 (0.8) −0.07 (0.8)
MEpink 0.49 (0.08) −0.49 (0.08)
MEpurple −0.37 (0.2) 0.37 (0.2)
MEred 0.73 (0.003) −0.73 (0.003)
MEroyalblue 0.51 (0.06) −0.51 (0.06)
MEsalmon −0.16 (0.6) 0.16 (0.6)
MEtan 0.1 (0.7) −0.1 (0.7)
MEturquoise 0.047 (0.9) −0.047 (0.9)
MEyellow −0.36 (0.2) 0.36 (0.2)
Con
Treat

Figure 7

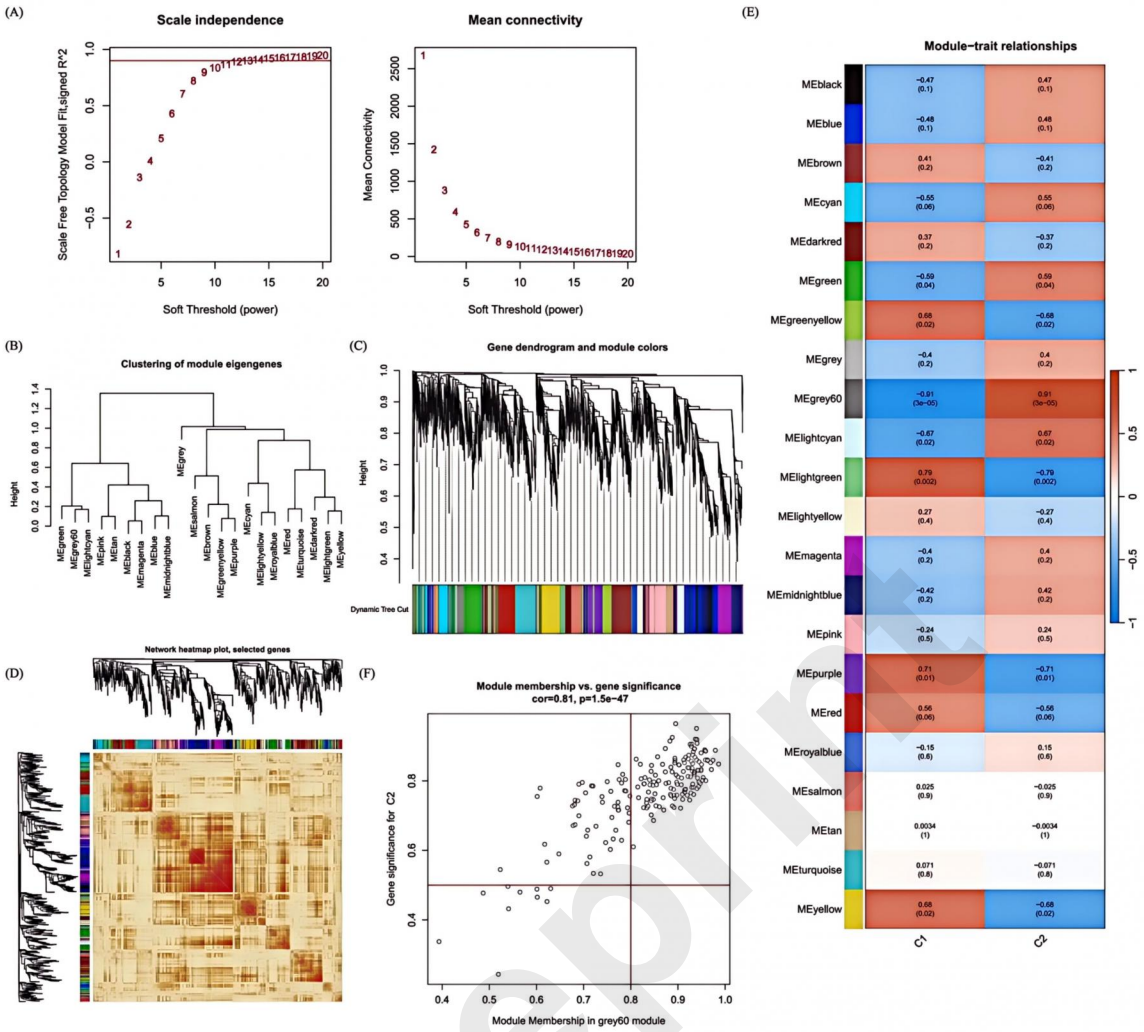

Figure 8

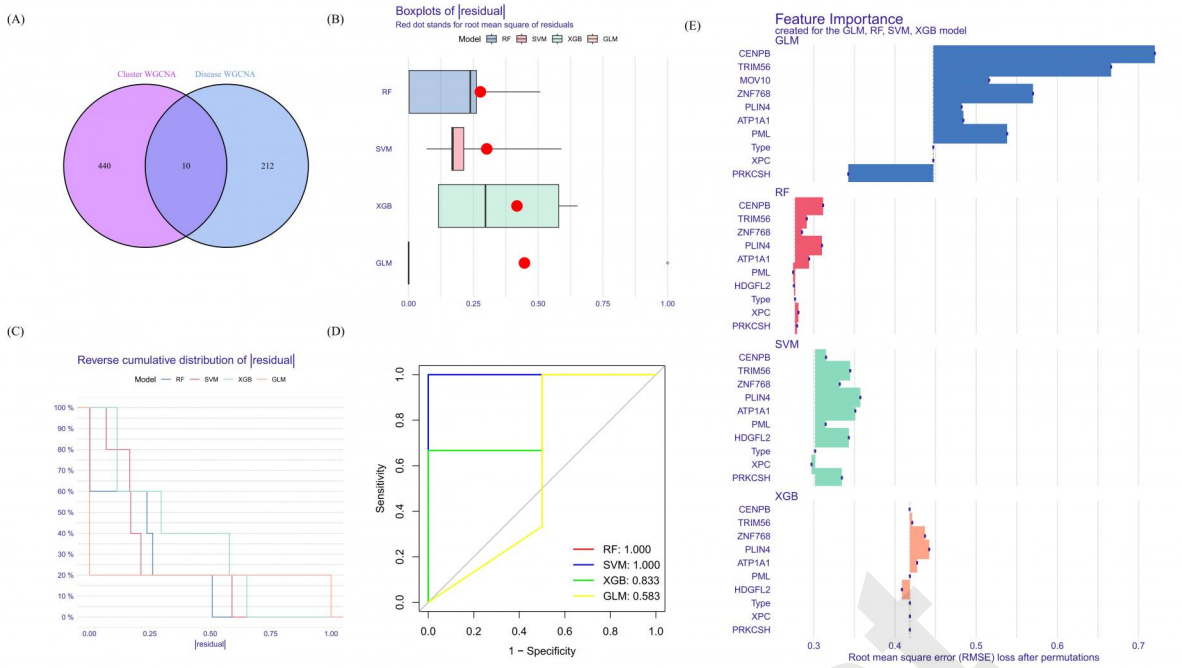

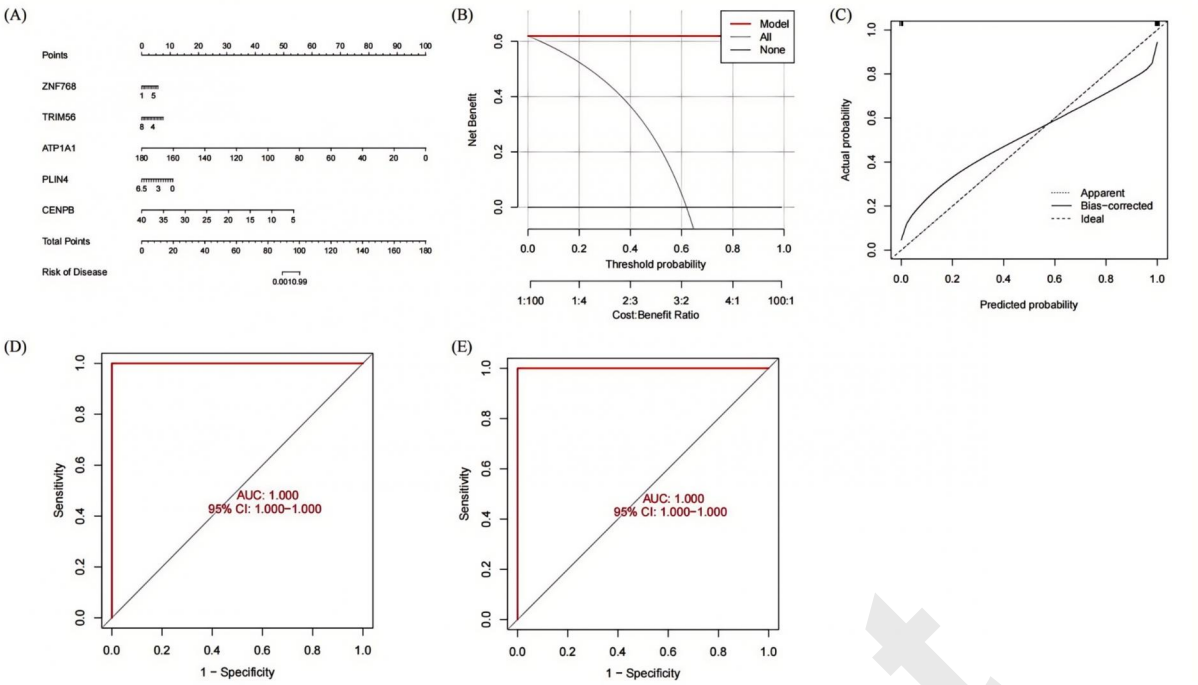
(A)
Points
ZNF768
TRIM56
ATP1A1
PLIN4
CENPB
Total Points
Risk of Disease
(B)
Model
All
None
Net Benefit
Threshold probability
Cost:Benefit Ratio
(C)
Actual probability
Predicted probability
Apparent
Bias−corrected
Ideal
(D)
Sensitivity
1 − Specificity
AUC: 1.000
95% CI: 1.000−1.000
(E)
Sensitivity
1 − Specificity
AUC: 1.000
95% CI: 1.000−1.000